

Optical Properties of Nanocrystal Interfaces in Compressed MgO Nanopowders

Keith P. McKenna,^{†,‡,*} David Koller,[§] Andreas Sternig,[†] Nicolas Siedl,^{§,†} Niranjan Govind,^{||} Peter V. Sushko,[‡] and Oliver Diwald^{§,†,*}

[†]WPI-AIMR, Tohoku University, 2-1-1, Katahira, Aoba-ku, Sendai 980-8577, Japan, [‡]Department of Physics and Astronomy, University College London, Gower Street, London WC1E 6BT, United Kingdom, [§]Institute of Materials Chemistry, Vienna University of Technology, Getreidemarkt 9, 1060 Wien, Austria, [†]Friedrich-Alexander Universitat, Erlangen-Nurnberg, Cauerstrasse 4, Erlangen D-91058, Germany, and ^{||}Environmental Molecular Sciences Laboratory, Pacific Northwest National Laboratory, 902 Battelle Boulevard, Richland, Washington 99352, United States

Powders of metal oxide nanocrystals find important applications in fields as diverse as catalysis,¹ medicine, cosmetics, and energy generation² owing to their unique and often tunable properties. A great deal of research has focused on understanding photoexcited processes in such nanopowders. When discussing how the spectroscopic properties and surface reactivity of nanopowders differ from those of macroscopic materials, it is common to point to their high specific surface area, the size and shape of the constituent nanocrystals, and the high concentration of surface features, such as steps, kinks, and other low coordination sites. Another defining characteristic of nanopowders is the large number of interfaces between nanocrystals they contain. However, the influence of interfaces on the overall optical properties of nanopowders has not so far been studied. As well as being an important issue for the aforementioned applications, understanding the role of interfaces is important for materials characterization, as in order to perform spectroscopic measurements, nanoparticle powders are often pressed into pellets, inevitably generating nanocrystal interfaces. Furthermore, understanding how interfaces affect optical properties may open the way to using optical spectroscopy as a probe of the electronic properties of interfaces between nanocrystals, which are thought to be important for effects such as magnetism in nanopowders,³ and for understanding the dynamics of electrons and holes under irradiation.^{4,5}

In this article, we combine experiment and first-principles theoretical calculations to investigate the optical properties of interfaces in metal oxide nanopowders. MgO provides a

ABSTRACT The optical properties and charge trapping phenomena observed on oxide nanocrystal ensembles can be strongly influenced by the presence of nanocrystal interfaces. MgO powders represent a convenient system to study these effects due to the well-defined shape and controllable size distributions of MgO nanocrystals. The spectroscopic properties of nanocrystal interfaces are investigated by monitoring the dependence of absorption characteristics on the concentration of the interfaces in the nanopowders. The presence of interfaces is found to affect the absorption spectra of nanopowders more significantly than changing the size of the constituent nanocrystals and, thus, leading to the variation of the relative abundance of light-absorbing surface structures. We find a strong absorption band in the 4.0–5.5 eV energy range, which was previously attributed to surface features of individual nanocrystals, such as corners and edges. These findings are supported by complementary first-principles calculations. The possibility to directly address such interfaces by tuning the energy of excitation may provide new means for functionalization and chemical activation of nanostructures and can help improve performance and reliability for many nanopowder applications.

KEYWORDS: nanocrystals · nanopowders · metal oxide · optical absorption · first-principles calculations

convenient reference system for this study due to its simple crystal structure, high thermal stability, and the possibility to produce nanocrystals with well-defined size and shape.^{6,7} Previous studies, using techniques such as electron paramagnetic resonance, optical spectroscopy, and first-principles calculations, have shown that MgO nanopowders exhibit optical absorption and luminescence bands that are red-shifted compared to the bulk.^{6–11} For example, the bulk absorption threshold for MgO is 7.7 eV, but lower energy bands are also observed in nanopowders, which have been attributed to surface features such as corners (4.6 eV) and edges (5.2 eV).^{7,9} The approach we have devised to investigate the optical properties of interfaces involves increasing their concentration by mechanical compaction of the nanopowder. We find two substantial changes in the

* Address correspondence to
k.mckenna@ucl.ac.uk;
o.diwald@fzg.uni-erlangen.de.

Received for review January 6, 2011
and accepted March 28, 2011.

Published online March 28, 2011
10.1021/nn200062d

© 2011 American Chemical Society

UV diffuse reflectance spectra of MgO nanopowders resulting from compaction: the emergence of new absorption features in the range 4.0–5.5 eV and a depression in intensity at 5.7 eV. With the help of complementary first-principles calculations, these changes are interpreted in terms of the excitation of nanocrystal interfaces. An important conclusion of our study is that photons with low energy, *e.g.*, 4.6 eV, excite electrons not only at MgO surfaces, as previously believed, but also at interfaces inside the powder. This is the first experimental evidence for the emergence of new electronic states that arise from the contact area between nanocrystals.

RESULTS AND DISCUSSION

MgO nanopowders were prepared using a chemical vapor synthesis (CVS) procedure based on metal vapor combustion with oxygen within a flow reactor system (see Methods section for details). We showed previously⁶ that by varying CVS parameters one can produce powders consisting of cubic nanocrystals with a well-defined size as small as 3 nm edge length. The, as-formed, powders were cleaned of organic contaminants by heating to 1123 K at a rate of 5 K min⁻¹ and exposing to molecular oxygen at this temperature. Then, the sample temperature was raised to 1173 K at pressures $p < 5 \times 10^{-6}$ mbar and kept at this temperature for 5 h until full dehydroxylation of the sample surface was achieved. This procedure forms low-density powders (less than 1% of the bulk MgO density, $\rho_{\text{MgO}} = 3580 \text{ kg m}^{-3}$), and transmission electron microscopy (TEM) demonstrates they consist of loosely agglomerated cubic nanocrystals.^{6,12} To obtain compressed MgO samples, a known mass of the powder is transferred into a 0.05 cm³ cavity and a hydraulic press is used to compact the powder. By varying the pressure applied, powders with a range of densities can be produced. The density of the compressed powder is determined from the known volume of the cavity after pressing. The pressed MgO pellet is then again subjected to a vacuum annealing procedure at 1173 K for 5 h, as well as annealing in 10 mbar of molecular oxygen at 1123 K for 10 min.

We now describe how the properties of the MgO nanopowder are modified by compaction. We will focus on the difference between the as-formed powder (<1% ρ_{MgO}) and a powder compressed to 50% of the bulk MgO density. We will hereafter refer to these two samples as loose and dense MgO powders, respectively. X-ray diffraction (XRD) confirms that both loose and dense powder samples are crystallized in the cubic rock salt phase (Figure 1a). The average nanocrystal size was determined from reflex broadening using the Debye–Scherrer equation. The loose powder contains nanocrystals of average diameter, 7.6 ± 1 nm, which is increased to 11.1 ± 1 nm in the dense powder. For the latter, analysis of the TEM images (Figure 1b)

shows that the edge length is most commonly distributed between 8 and 12 nm (Supporting Information, Figure S1), consistent with the XRD analysis. To determine the specific surface area (S_{BET}), we measured N₂ adsorption isotherms (Supporting Information, Figures. S2a and S2b) and applied the Brunauer, Emmett, and Teller (BET) model.¹³ The analysis shows a reduction in specific surface area from 303 m² g⁻¹ for the loose powder to 108 m² g⁻¹ for the dense powder. Applying the Barret, Joyner, and Halenda model¹⁴ to the N₂ adsorption isotherms also allows one to obtain the pore size distributions. Figure 1c shows that in the case of the loose powder we have a broad pore size distribution, which is consistent with a loosely connected powder with few nanocrystal interfaces. In the case of the dense powder, the pore distribution is peaked at approximately 10 nm, suggesting that a particle network containing numerous interfaces has been formed.

Part of the 195 m² g⁻¹ reduction in specific surface area that is observed following compaction is a consequence of the increased nanocrystal size. Another important factor is the formation of areas of contact between nanocrystals in the compressed powder, which leads to increased interface area at the expense of surface area. Finally, internal voids that are inaccessible to N₂ may be present, which would also contribute to the observed reduction. Given the relatively high porosity of the two powder samples, the contribution from internal voids is expected to be small and is neglected in the following analysis. To help separate the remaining two contributions, we have calculated the specific surface area of nanocrystals using the average edge length determined by XRD (d_{XRD}). For this calculation, we assume isolated cubic nanocrystals and use the following expression: $S = 6/d_{\text{MgO}}$ (Table 1). Direct comparison between the XRD- and BET-determined surface areas is difficult due to the different types of approximation that are involved¹⁵ (see Supporting Information). However, since for the loose powder we expect the assumption of isolated cubic nanocrystals to be valid, we can obtain a normalizing factor by equating S_{XRD} and S_{BET} for the loose powder. In this way, the difference ($S_{\text{XRD}} - S_{\text{BET}}$) provides a proportional measure of the interface area (Figure 1d, Table 1). From this analysis, we determine that the area associated with interfaces between nanocrystals is approximately 100 m² g⁻¹ in the dense powder. In other words, ~50% of the nanocrystal surfaces in the dense powder are in direct contact with other nanocrystals.

Figure 2a compares the UV diffuse reflectance spectra acquired for loose nanopowder samples (with $d_{\text{XRD}} = 7.6$ nm and $d_{\text{XRD}} = 10.0$ nm) and for a dense nanopowder sample ($d_{\text{XRD}} = 11.1$ nm). The relative intensity of the absorption bands in these spectra reflect the relative proportion of the associated structural features

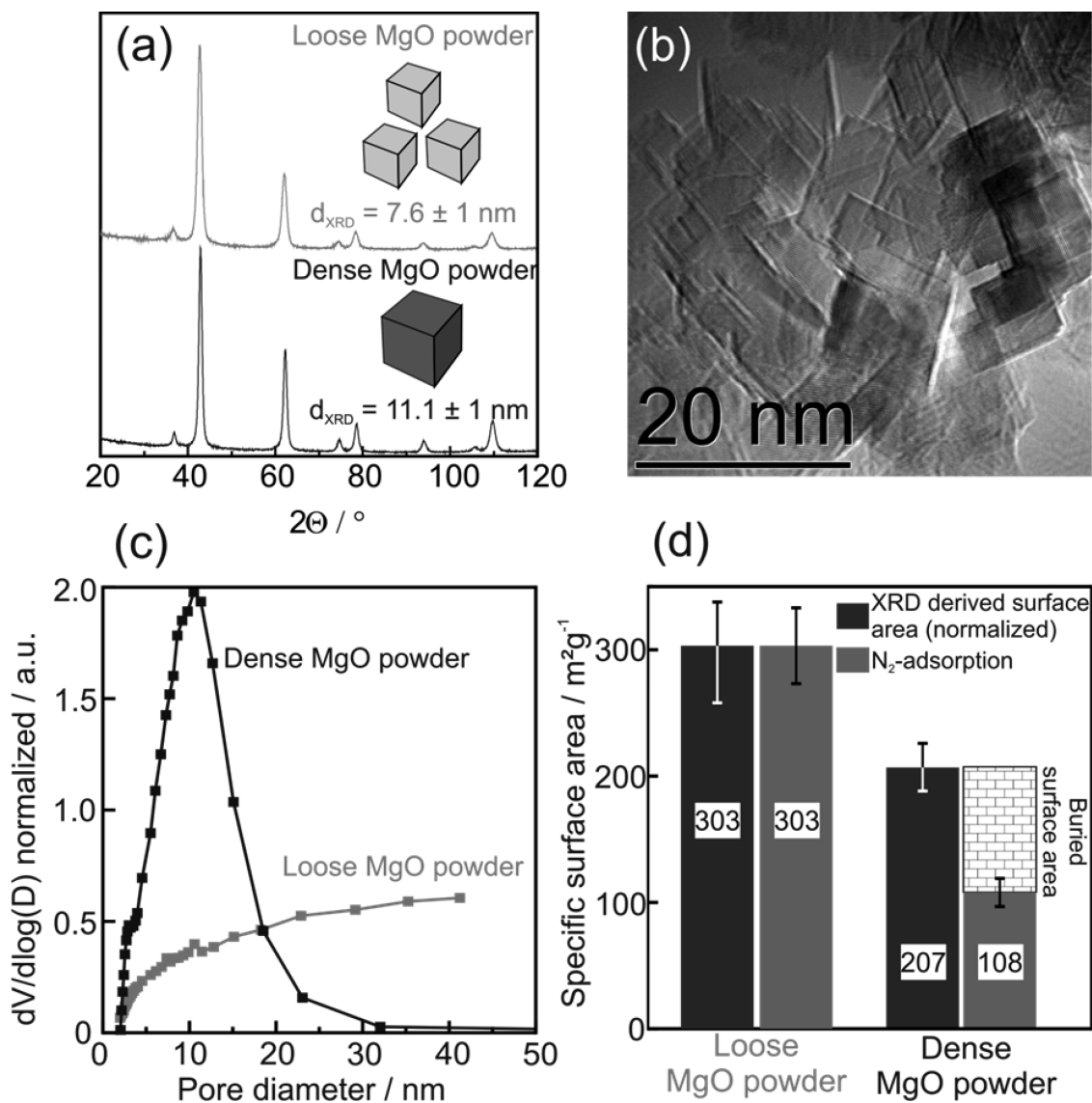


Figure 1. (a) XRD patterns of loose and dense MgO powder with corresponding average nanocrystal size. (b) Electron microscopy images of CVS-MgO after applying uniaxial pressure of $1.7 \times 10^8 \text{ Pa}$ and subsequent thermal annealing ($T = 1170 \text{ K}$, $p < 10^{-6} \text{ mbar}$). (c) Distribution in pore sizes for the loose and dense powder as determined from analysis of N_2 -adsorption isotherms. (d) Corrected specific surface area either derived from the average nanocrystal sizes or directly determined from the N_2 -adsorption isotherms.

TABLE 1. Average Nanocrystal Sizes Determined Using the Debye–Scherrer Equation (d_{XRD}), Specific Surface Area Calculated from Average Nanocrystal Sizes (S_{XRD}), Specific Surface Area Determined from N_2 Adsorption (S_{BET}), and the Resulting Interface Area

	loose powder	dense powder
d_{XRD} (nm)	7.6 ± 1	11.1 ± 1
S_{XRD} ($\text{m}^2 \text{g}^{-1}$)	221	151
normalized S_{XRD} ($\text{m}^2 \text{g}^{-1}$)	303	207
S_{BET} ($\text{m}^2 \text{g}^{-1}$)	303 ± 30	108 ± 11
interface area ($S_{XRD} - S_{BET}$) ($\text{m}^2 \text{g}^{-1}$)	99	

responsible for the excitations. For example, for loose powders, previous studies have shown that the 4.6 and 5.2 eV bands are associated with low-coordinated corner and edge ions, respectively.^{6,11} As the size of the

nanocrystals increases, the concentration of corner ions is decreased, explaining why the absorption band at 4.6 eV is essentially absent for the 10 nm loose powder (bottom trace in Figure 2a). However, slightly larger compressed MgO nanopowders exhibit UV absorption that extends significantly into the energy range below 5.0 eV, indicating substantial changes in the electronic structure induced by the introduction of nanocrystal interfaces. By taking the difference between the two spectra (10 nm loose and 11.1 nm dense), one can separate out the effects of interfaces. Figure 2b shows that as the density increases, a band of excitations in the range 4.0–5.5 eV increases in intensity, while the intensity of a band at 5.7 eV decreases. The differences between the absorption spectra show that the effect of the interfaces in the range 4.0–5.5 eV is much

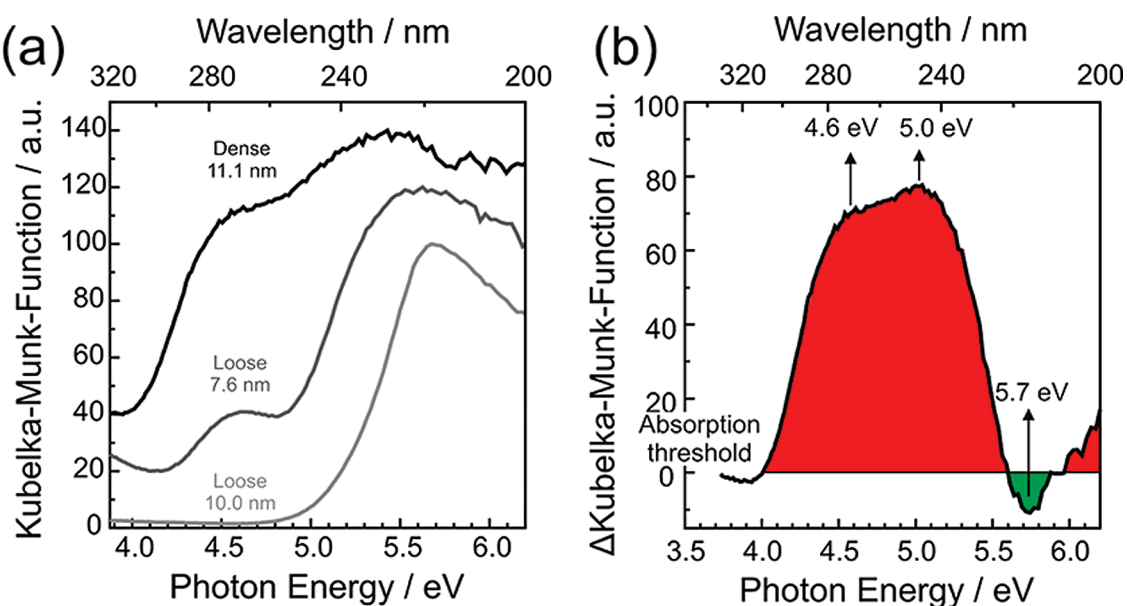


Figure 2. (a) Experimental UV diffuse reflectance spectra for loose and dense MgO powder samples. Average crystallite sizes (shown) were determined applying the Debye–Scherrer equation to XRD powder patterns. The spectra are displaced vertically for clarity. (b) Difference between the spectra obtained for 10.0 nm loose and 11.1 nm dense MgO powders.

stronger than the effect of the nanocrystal size (see Figure 2 and Figure S4, Supporting Information). Residual surface hydroxyls can be excluded as the origin of the emerging bands, because—if present—such adsorbates would decrease the sample absorption in this energy range rather than increasing it (see Supporting Information). Some of the new bands introduced by interfaces overlap with bands that were previously thought to selectively excite only low-coordinated surface ions.

On the basis of our experimental structural characterization, we adopt the model of powder densification shown in Figure 3a.^{16–19} The main effect of compression and annealing is to reduce the size of voids in the powder by forcing the nanocrystals to reorganize, forming a more dense network containing more interfaces in the process. This can involve a number of interrelated processes such as rotation and translation of nanocrystals, mass transfer between the nanocrystals resulting in size change, and growth of grain boundaries between nanocrystals. Following this transformation the constituent nanocrystals remain cubic and crystalline, and there is an increase in their average size, indicating some degree of sintering. It is difficult to extract the structure of interfaces present in the nanopowders directly from the experimental measurements. However, it is expected that the most common type of interface between cubic MgO nanocrystals will involve the commensurate contact between their (001) facets. The reasons for this are as follows: (1) commensurate interfaces are the most stable thermodynamically; (2) they seem to be common in TEM images of nanopowders,²⁰ and (3) previous TEM studies on larger MgO smoke particles deposited onto a MgO substrate found a clear

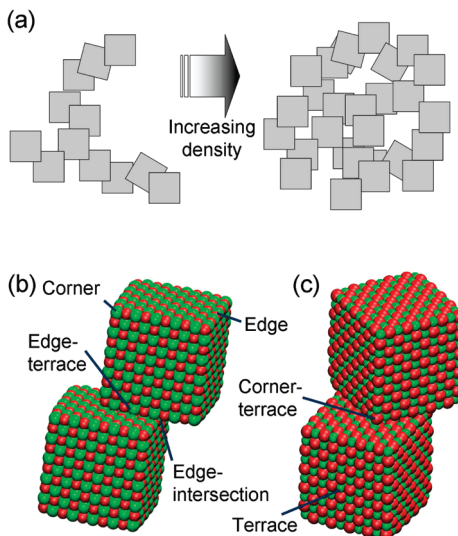


Figure 3. (a) Model for changes in powder structure on compression. (b) Structural features at the interface between nanocrystals that are commensurate or (c) rotated with respect to each other.

preference for commensurate interfaces.²¹ In this latter study, a smaller fraction of interfaces were also found to be rotated (corresponding to high site coincidence twist grain boundaries).

To provide atomistic models for interfaces in the MgO powders, we performed theoretical calculations of some possible metastable configurations of two adjoining MgO nanocrystals. These calculations considered nanocrystals containing 1000 ions and described the interionic bonding using the classical shell model.²² The two cubic MgO nanocrystals were initially oriented and translated with respect to each other before relaxing

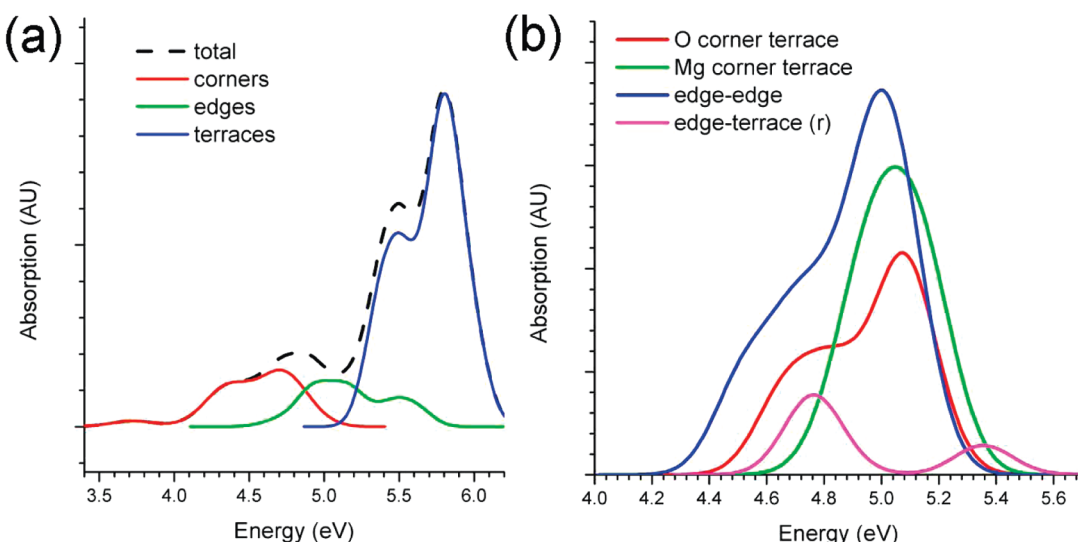


Figure 4. (a) Theoretically simulated spectra for loose powder assuming dominant contributions from corners, edges, and terraces and (b) excitation spectra for various interface features formed between commensurate and rotated (r) nanocrystals.

the structure into various local energy minima. An alternative approach would be to employ molecular dynamics to simulate the sintering of nanocrystals, as has been done recently for TiO_2 .²³ Figure 3b,c shows examples of both a commensurate and a rotated interface that contain various structural features. For example, the corner–terrace feature is formed at the contact point between the corner of one nanocrystal and the (001) terrace of another. In addition to features formed at contact points between nanocrystals, the surface features of individual nanocrystals (*i.e.*, the corner, edge, and terrace) are indicated. While, in general, the structure of nanopowders may be quite complicated, we expect they should be predominantly built from these fundamental structural features. Therefore, these models form the basis for the first-principles calculations that are used to help interpret the experimentally determined absorption spectra.

Excitation spectra have been calculated using time-dependent density functional theory (TD-DFT) implemented within an embedded cluster method. To calculate excitation spectra for the various features identified in Figure 3b,c, quantum clusters were constructed that were sufficiently large to ensure accurate description of the surface and interface electronic states participating in the electronic transitions. The largest system we considered contained 73 atoms treated at an all-electron level (730 electrons in total), spanning a region of $\sim 1 \text{ nm}^3$, which was described using 1723 basis functions (see Supporting Information for more details). For this cluster, we computed 50 excited states using TD-DFT, a calculation that was possible only through the use of the highly parallelized NWChem code.²⁴

The excitation spectra of the loose powder is simulated by assuming it to be dominated by the excitation of corner, edge, and terrace features. To obtain the

total excitation spectra, we sum up the individual contributions weighted in proportion to the number of corner, edge, and terrace sites in the powder. One can either determine these weights from atomistic models or use them as fitting parameters if comparing to an experimental spectrum. Figure 4a (dashed curve) shows the simulated spectra of an isolated 2 nm nanocrystal, where we used the proportion of various surface sites appropriate for cubic nanocrystals.⁶ In this spectra, one can identify a very weak feature at 3.7 eV and a more intense peak at 4.7 eV. Both of these features are associated with localized excitations at corner ions. At higher energies, contributions from edges in the range 5.0–5.5 eV partly overlap with terrace excitations peaking near 5.8 eV. This simulated spectrum provides very good agreement with the measured spectrum for the loose powder (Figure 2a). To test our hypothesis that the experimentally observed difference spectra are due to the increased number of interfaces in the dense powder, we calculate the excitation spectra of various structural features formed at the interface between MgO nanocrystals, including corner–terrace, edge–terrace, and edge–intersection features (as shown in Figure 3b,c). All interfaces considered contribute excitations in the range 4.4–5.4 eV (Figure 4b), consistent with the experimental result. Furthermore, as the density increases, the total area of free terrace is reduced (as shown by N_2 -sorption measurements); therefore, one should expect a reduction in the intensity associated with terraces. The calculations predict that this depression will occur at 5.8 eV (*i.e.*, the position of the peak in absorption due to terraces, Figure 2a, again in close agreement with experiment (5.7 eV)).

On the basis of the combined experimental and theoretical investigation, we find that a wide range of interfaces in MgO nanopowders, even those that are

highly coordinated, can contribute low-energy excitations in the 4.0–5.5 eV range. The theoretical calculations explain the origin of this effect. At interfaces, there is a significant perturbation in the structure, and as a consequence, the Madelung potential on interface ions can be significantly reduced. For example, the Madelung potential near the corner–terrace feature is up to 0.5 V lower than at the free edge. It is this electrostatic perturbation that is responsible for the presence of interfacial electronic states and gives rise to excitation energies significantly lower than those of isolated particles. For example, one of the dominant excitations for the edge–intersection feature at 4.7 eV involves transition of an electron from oxygen p-states on the edge of one cube to the edge of the adjacent cube. This novel type of interparticle excitation may have interesting consequences, for example, leading to the development of nonequilibrium electric fields within nanopowders under irradiation. It has been proposed that such electric fields may weaken chemical bonds in small molecules and, therefore, facilitate chemical reactions between them.^{25,26}

In summary, we have shown, by monitoring the optical properties of a nanopowder as the density of

the powder is increased, how one can determine the excitation/absorption characteristics of interfaces. While we have considered MgO as a model system, the results suggest that understanding exciton generation at interfaces, and the associated electron–hole dynamics, may be important for other materials and applications. By combining theory and experiment one can identify regions of the spectra that are associated with particular types of interface. The possibility to directly address such interfaces by tuning the energy of excitation is key to understanding exciton generation at interfaces and associated charge separation. Moreover, it may provide new means for functionalization of nanostructures and chemical activation and can help improve performance and reliability for many nanopowder applications, such as photocatalysts and solar cells. For example, there is considerable interest in porous nanocrystalline ceramics for catalytic applications,^{27,28} batteries, solar cells,²⁹ and gas sensing, where interfaces may play an important role. The key result of this study is that the effect of interfaces in powders of ionic nanocrystals on the optical properties may be as important as those specific for low-coordinated adsorption sites.

METHODS

For the production of MgO nanocrystals we use chemical vapor synthesis, which allows for the controlled evaporation and subsequent oxidation of alkaline earth metals under reduced pressures.^{30,31} Further details can be found in the Supporting Information. After production, the MgO nanocrystal powder is transferred into quartz glass cells, which allow one to carry out thermal activation of the nanocrystal powders in defined gas atmospheres on one hand and spectroscopy measurements on the other. To obtain well-defined cubic MgO nanocrystals, the as-obtained MgO powder is cleaned of organic contaminants by heating to 1123 K at a rate of 5 K min⁻¹ and exposing to molecular oxygen at this temperature. Then, the sample temperature was raised to 1173 K at pressures $p < 5 \times 10^{-6}$ mbar and kept at this temperature for 5 h until full dehydroxylation of the sample surface was achieved.

X-ray diffraction patterns were collected on a PANalytical X'Pert PRO diffractometer using Cu K α radiation. The nanocrystal sizes were derived on the basis of the Debye–Scherrer equation with the assumption of cubically shaped nanocrystals. We used pseudo-Voigt functions to determine the full width half-maximum of the three main reflexes to calculate an average nanocrystal size (d_{XRD}).

To obtain the transmission electron microscopy images, small amounts of the metal oxide powders were cast on a holey carbon grid for investigation with a TECNALI F20 analytical transmission electron microscope equipped with a field emission gun and an S-twin objective lens.

Nitrogen adsorption isotherms were obtained at 77 K using an adsorption porosimeter (Micromeritics ASAP 2020). Samples were outgassed for 6 h in the degas unit of the adsorption apparatus at 473 K under vacuum prior to analysis. The BET surface area (S_{BET}) was evaluated using adsorption data in a relative pressure range p/p_0 of 0.05–0.2.

UV diffuse reflectance spectra for the loose and dense powders were acquired in the presence of 10 mbar of O₂ using a PerkinElmer Lambda 15 spectrophotometer, equipped with an integrating sphere, and then converted to absorption spectra by the Kubelka–Munk transform procedure. There are

differences in the absolute light penetration depth due to the different densities of the samples; therefore, reported spectra are normalized with respect to their maximum reflectance value.

Excitation spectra have been calculated using time-dependent density functional theory implemented within an embedded cluster method. This technique consistently combines quantum mechanical and classical methods to enable large systems to be studied and to ensure accurate description of long-range polarization effects. Classical ions are described using empirical pair potentials,²² and quantum mechanical ions are treated using the B3LYP hybrid density functional³² and the Gaussian 6-311G* basis set. This method is implemented in the Guess code,¹⁰ which was interfaced with the NWChem code^{24,33} for the quantum mechanical part of the calculation.

Acknowledgment. The experimental part of this project has been financially supported by Fonds zur Förderung der Wissenschaftlichen Forschung (FWF) P19848-N20, which is gratefully acknowledged by D.K., A.S., N.S., and O.D. K.M. acknowledges support from MEXT KAKENHI project number 2274019 and helpful discussions with A. Shluger. P.V.S. is supported by the Royal Society and the JSPS First program. The TEM image in Figure 1b was kindly provided by Dr. Johannes Bernardi (Vienna University of Technology, USTEM). N.G. acknowledges support from the EMSL Intramural Program. The embedded cluster calculations were performed using the NWChem/Guess program on the Chinook supercomputer at EMSL, a national scientific user facility sponsored by the Department of Energy's Office of Biological and Environmental Research and located at Pacific Northwest National Laboratory. This work also made use of the facilities of HECToR, the UK's national high-performance computing service, via our membership in the UK's HPC Materials Chemistry Consortium, which is funded by EPSRC (EP/F067496).

Supporting Information Available: Structural characterization, absorption spectra measurements, and theoretical models. This material is available free of charge via the Internet at <http://pubs.acs.org/>.

REFERENCES AND NOTES

- Fox, M. A.; Dulay, M. T. Heterogeneous Photocatalysis. *Chem. Rev.* **1993**, *93*, 341–357.
- Péchy, P.; Renouard, T.; Zakeeruddin, S. M.; Humphry-Baker, R.; Comte, P.; Liska, P.; Cevey, L.; Costa, E.; Shklover, V.; Spiccia, L.; et al. Engineering of Efficient Panchromatic Sensitizers for Nanocrystalline TiO₂-Based Solar Cells. *J. Am. Chem. Soc.* **2001**, *123*, 1613–1624.
- Stoneham, M. The Strange Magnetism of Oxides and Carbons. *J. Phys.: Condens. Matter* **2010**, *22*, 074211.
- McKenna, K. P.; Sushko, P. V.; Shluger, A. L. Inside Powders: A Theoretical Model of Interfaces between MgO Nanocrystallites. *J. Am. Chem. Soc.* **2007**, *129*, 8600–8608.
- McKenna, K. P.; Shluger, A. L. Electron-Trapping Polycrystalline Materials with Negative Electron Affinity. *Nat. Mater.* **2008**, *7*, 859–862.
- Stankic, S.; Müller, M.; Diwald, O.; Sterrer, M.; Knözinger, E.; Bernardi, J. Size-Dependent Optical Properties of MgO Nanocubes. *Angew. Chem., Int. Ed.* **2005**, *44*, 4917–4920.
- Stankic, S.; Bernardi, J.; Diwald, O.; Knözinger, E. Optical Surface Properties and Morphology of MgO and CaO Nanocrystals. *J. Phys. Chem. B* **2006**, *110*, 13866–13871.
- Sterrer, M.; Diwald, O.; Knözinger, E.; Sushko, P. V.; Shluger, A. L. Energies and Dynamics of Photoinduced Electron and Hole Processes on MgO Powders. *J. Phys. Chem. B* **2002**, *106*, 12478–12482.
- Sternig, A.; Müller, M.; McCallum, M.; Bernardi, J.; Diwald, O. BaO Clusters on MgO Nanocubes: A Quantitative Analysis of Optical-Powder Properties. *Small* **2010**, *6*, 582–588.
- Sushko, P. V.; Shluger, A. L.; Catlow, C. R. A. Relative Energies of Surface and Defect States: *ab initio* Calculations for the MgO (001) Surface. *Surf. Sci.* **2000**, *450*, 153–170.
- Sushko, P. V.; Gavartin, J. L.; Shluger, A. L. Electronic Properties of Structural Defects at the MgO (001) Surface. *J. Phys. Chem. B* **2002**, *106*, 2269–2276.
- Sternig, A.; Stankic, S.; Müller, M.; Bernardi, J.; Knözinger, E.; Diwald, O. Photoluminescent Nanoparticle Surfaces: The Potential of Alkaline Earth Oxides for Optical Applications. *Adv. Mater.* **2008**, *20*, 4840–4844.
- Brunauer, S.; Emmett, P. H.; Teller, E. Adsorption of Gases in Multimolecular Layers. *J. Am. Chem. Soc.* **1938**, *60*, 309–319.
- Barrett, E. P.; Joyner, L. G.; Halenda, P. P. The Determination of Pore Volume and Area Distributions in Porous Substances. I. Computations from Nitrogen Isotherms. *J. Am. Chem. Soc.* **1951**, *73*, 373–380.
- Weibel, A.; Bouchet, R.; Boulc'h, F.; Knauth, P. The Big Problem of Small Particles: A Comparison of Methods for Determination of Particle Size in Nanocrystalline Anatase Powders. *Chem. Mater.* **2005**, *17*, 2378–2358.
- Lange, F. F. Powder Processing Science and Technology for Increased Reliability. *J. Am. Ceram. Soc.* **1989**, *72*, 3–15.
- Hütter, M. Local Structure Evolution in Particle Network Formation Studied by Brownian Dynamics Simulation. *J. Colloid Interface Sci.* **2000**, *231*, 337–350.
- van de Lagemaat, J.; Benkstein, K. D.; Frank, A. J. Relation between Particle Coordination Number and Porosity in Nanoparticle Films: Implications to Dye-Sensitized Solar Cells. *J. Phys. Chem. B* **2001**, *105*, 12433–12436.
- Benkstein, K. D.; Kopidakis, N.; van de Lagemaat, J.; Frank, A. J. Influence of the Percolation Network Geometry on Electron Transport in Dye-Sensitized Titanium Dioxide Solar Cells. *J. Phys. Chem. B* **2003**, *107*, 7759–7767.
- Nowak, J.; Carter, C. Forming Contacts and Grain Boundaries between MgO Nanoparticles. *J. Mater. Sci.* **2009**, *44*, 2408–2418.
- Chaudhari, P.; Matthews, J. W. Coincidence Twist Boundaries between Crystalline Smoke Particles. *J. Appl. Phys.* **1971**, *42*, 3063–3066.
- Lewis, G. V.; Catlow, C. R. A. Potential Models for Ionic Oxides. *J. Phys. C: Solid State Phys.* **2004**, *18*, 1149–1161.
- Alimohammadi, M.; Fichthorn, K. A. Molecular Dynamics Simulation of the Aggregation of Titanium Dioxide Nanocrystals: Preferential Alignment. *Nano Lett.* **2009**, *9*, 4198–4203.
- Valiev, M.; Bylaska, E.; Govind, N.; Kowalski, K.; Straatsma, T.; Dam, H. V.; Wang, D.; Nieplocha, J.; Apra, E.; Windus, T.; et al. NWChem: A Comprehensive and Scalable Open-Source Solution for Large Scale Molecular Simulations. *Comput. Phys. Commun.* **2010**, *181*, 1477–1489.
- Grimme, S.; Kruse, H.; Goerigk, L.; Erker, G. The Mechanism of Dihydrogen Activation by Frustrated Lewis Pairs Revisited. *Angew. Chem., Int. Ed.* **2010**, *49*, 1402–1405.
- Kathmann, S. M.; Kuo, I.-F. W.; Mundy, C. J.; Schenter, G. K. Understanding the Surface Potential of Water. *J. Phys. Chem. B* **2011**, dx.doi.org/10.1021/jp1116036.
- Richards, R.; Li, W.; Decker, S.; Davidson, C.; Koper, O.; Zaikovski, V.; Volodin, A.; Rieker, T.; Klabunde, K. J. Consolidation of Metal Oxide Nanocrystals. Reactive Pellets with Controllable Pore Structure That Represent a New Family of Porous, Inorganic Materials. *J. Am. Chem. Soc.* **2000**, *122*, 4921–4925.
- Siedl, N.; Elser, M.; Bernardi, J.; Diwald, O. Functional Interfaces in Pure and Blended Oxide Nanoparticle Networks: Recombination versus Separation of Photogenerated Charges. *J. Phys. Chem. C* **2009**, *113*, 15792–15795.
- Hagfeldt, A.; Boschloo, G.; Sun, L.; Kloo, L.; Pettersson, H. Dye-Sensitized Solar Cells. *Chem. Rev.* **2010**, *110*, 6595–6663.
- Knözinger, E.; Diwald, O.; Sterrer, M. Chemical Vapour Deposition—A New Approach to Reactive Surface Defects of Uniform Geometry on High Surface Area Magnesium Oxide. *J. Mol. Catal. A* **2000**, *162*, 83–95.
- Knözinger, E.; Jacob, K. H.; Singh, S.; Hofmann, P. Hydroxyl Groups as IR Active Surface Probes on MgO Crystallites. *Surf. Sci.* **1993**, *290*, 388–402.
- Becke, A. D. Density-Functional Thermochemistry. III. The Role of Exact Exchange. *J. Chem. Phys.* **1993**, *98*, 5648–5652.
- Govind, N.; Sushko, P.; Hess, W.; Valiev, M.; Kowalski, K. Excitons in Potassium Bromide: A Study using Embedded Time-Dependent Density Functional Theory and Equation-of-Motion Coupled Cluster Methods. *Chem. Phys. Lett.* **2009**, *470*, 353–357.